

# Modified effective-range theory for low energy $e$ - $N_2$ scattering

Z. Idziaszek<sup>1,a</sup> and G. Karwasz<sup>2</sup>

<sup>1</sup> Instytut Fizyki Teoretycznej, Uniwersytet Warszawski, 00-681 Warszawa, Poland

<sup>2</sup> Instytut Fizyki, Uniwersytet Mikołaja Kopernika, 87-100 Toruń, Poland

Received 5 September 2008 / Received in final form 19 December 2008

Published online 6 February 2009 – © EDP Sciences, Società Italiana di Fisica, Springer-Verlag 2009

**Abstract.** We analyze the low-energy  $e$ - $N_2$  collisions within the framework of the modified-effective range theory (MERT) for the long-range potentials, developed by O'Malley et al. [J. Math. Phys. **2**, 491 (1961)]. In comparison to the traditional MERT we do not expand the total cross-section in the series of the incident momentum  $\hbar k$ , but instead we apply the exact analytical solutions of the Schrödinger equation for the long-range polarization potential, as proposed in the original formulation of O'Malley et al. This extends the applicability of MERT up to few eV regime, as we confirm using some simplified model potential of the electron-molecule interaction. The parameters of the effective-range expansion (i.e. the scattering length and the effective range) are determined from experimental, integral elastic cross-sections in the 0.1–1.0 eV energy range by fitting procedure. Surprisingly, our treatment predicts a shape resonance that appears slightly higher than experimentally well known resonance in the total cross-section. Agreement with the experimentally observed shape-resonance can be improved by assuming the position of the resonance in a given partial wave. Influence of the quadrupole potential on resonances is also discussed: we show that it can be disregarded for  $N_2$ . In conclusion, the modified-effective range formalism treating the long-range part of the potential in an exact way, reproduces well both the very low-energy behavior of the integral cross-section as well as the presence of resonances in the few eV range.

**PACS.** 34.80.Bm Elastic scattering

## 1 Introduction

Combining the short and long-term interactions is the classical problem of electron-molecule scattering theory. The widely used R-matrix method [1,2], for instance, applies two distinct methodologies, quantum chemistry and long-range interactions for inner and outer regions, respectively. Other approaches, like that by Czuchaj and collaborators for noble gases [3] use analytic short-range modifications to the polarization potential (we skip many other similar attempts). Even full ab-initio models use “effective core potential” [4,5]. Systematic studies of short-range effects, including the exact exchange and correlations potentials have been done for atomic and molecular targets by Gianturco and collaborators [6,7]. They showed, both for electron and positron scattering [8,9] how the low-energy cross-sections are sensitive to a proper choice of the cut-off parameters defining the inner and outer regions.

In our previous paper on positron-atom scattering [10] we have revisited a textbook formulation of the long and short range problem: the modified effective range theory (MERT) [11]. Analyzing the low-energy scattering on Ar and  $N_2$  targets, we have concluded that MERT expansion performed solely on the short-range part of the poten-

tials, reproduces well the experimental data up to few eV regime. Similar approach has been used in [12], to study both electron and positron scattering on  $CO_2$ , where we have shown that MERT, apart from the zero-energy limit, is able to reproduce approximately the position of the shape resonance at few eV. In the present paper we apply MERT to yet another, classical subject of the electron-molecule scattering: the  $N_2$  molecule in the low-energy region, where the well-known shape resonance appears in total and vibrational-excitation cross-sections (see for example [13–15]). Shortly, the present approach uses experimental elastic cross-sections in the very low-energy range (below 1 eV), see Karwasz et al. [16] to derive the scattering potential within the MERT formulation and then calculates the integral cross-section at energies up to 10 eV.

In MERT approach the scattering is due to the polarization potential and the short range potential is modelled by an effective range expansion. These features make MERT particularly suitable for the near-to-zero energy range, treated with difficulties in other approaches [17,18]. The near-to-zero energy MERT expansion continues to be applied to numerous problems: integral cross-sections for atoms [19,20], non-polar [21,22] and polar molecules [23,24]. MERT is frequently used by experimentalists for extrapolation of measured differential

<sup>a</sup> e-mail: idziaszek@fuw.edu.pl

and integral cross-sections towards energies and angles inaccessible by experiment [25–27]. Different extensions of MERT, consisting in developing phase shifts (or elements of the reactance,  $K$  matrix) into series of  $k$  were applied by Morrison et al. [17] to rotational excitation of  $N_2$  molecule, and by Macri and Barrachina to electron-metastable He scattering and electron photodetachment from  $Li^-$  [28,29].

The most extensive, to our knowledge, analysis of MERT applicability in electron scattering was done for noble gases by Buckman and Mitroy [30]. They concluded that MERT fails above about 1 eV, exact energy depending on the target. However, in that as well in numerous other MERT applications, those were integral cross-sections which were developed directly in series of the colliding electron momentum  $k$ . As we showed in the previous work [10], the range of applicability of such a series is limited to a few tenths of eV. Therein [10] we have investigated an alternative way of applying MERT, that closely follows the original formulation of O'Malley et al. [11]. It consists in calculating the phase shifts due to the polarization potential from Mathieu solutions of the Schrödinger equation and introducing the effective-range expansion *exclusively for the short-range potential*. There is no explicit  $k$  expansion for the integral cross-sections in our approach; only the short-range contribution expressed in terms of an appropriate boundary condition, is expressed as series of  $k$ . This makes the numerical procedures more complicated but has allowed to extend the applicability of MERT for positron-argon and -nitrogen scattering to the range of 2–3 eV. We note that our method closely resembles quantum-defect-theory formulation of the scattering problem, where the quantum-defect parameter, that slowly varies with energy, is expanded in a series of  $k$  (see e.g. [31]). In electron-atom scattering the quantum-defect theory has been already applied by Watanabe and Greene [32] to analyze photodetachment process of  $K^-$  and by Fabrikant [33] to low-energy electron-metal atoms resonances.

In this paper we apply our MERT-based model to the molecule  $N_2$ , well studied by beam and swarm techniques at energies down to less than 0.1 eV. The parameters of MERT expansion for the short-range potential are derived from fitting procedure using the recommended [16] integral cross-sections below 1 eV. Next, we use these potentials to calculate cross-section up to 10 eV, observing a broad  $p$ -wave resonance around 6 eV. In such an unconstrained fit the resonances appear at higher energies than experimental values. By small, within the experimental error bar, modifications of the data used for the inversion procedure, one can reproduce the exact position of the resonances. In that case both resonances appearing in the  $p$  or  $d$ -partial wave channels are narrower than experimentally determined (but this can be partially caused by neglecting the nuclear motion, see for ex. reference [48]). We discuss also the relative contributions to integral cross-sections from the non-spherical part of the polarizability and the quadrupole moment of molecule, using the distorted-wave approximation.

The paper is organized as follows. In Section 2 we discuss the analytical solutions of the Schrödinger equation with the polarization potentials, and we present principles of the modified effective-range expansion. In Section 3 we demonstrate that MERT can describe both low-energy part and shape resonances in  $p$ - and  $d$ -wave cross-sections, assuming some simplified model of electron-molecule potential. The actual electron resonance in  $N_2$  is analyzed in Section 4. Section 5 discusses correction to MERT cross-sections due to the non-spherical part of the polarization potential and the molecule quadrupole moment. We present some conclusions in Section 6. Finally, three appendices give some technical details of the analytical solutions for the polarization potential.

## 2 Scattering of a charged particle on a molecule and the quantum-defect approach

The relative motion of a charged particle and a non-polar molecule is described by the Schrödinger equation

$$\left[ -\frac{\hbar^2}{2\mu}\Delta + V(\mathbf{r}) - E \right] \Psi(\mathbf{r}) = 0, \quad (1)$$

where  $\mu$  is the reduced mass,  $E$  is the relative energy of the particles, and  $V(\mathbf{r})$  is the particle-molecule potential. Potential  $V(\mathbf{r})$  can be written as a sum

$$V(\mathbf{r}) = V_1(\mathbf{r}) + V_2(\mathbf{r}) + V_S(r) \quad (2)$$

of long-range contributions

$$V_1(\mathbf{r}) = -\frac{\alpha e^2}{2r^4} \quad (3)$$

$$V_2(\mathbf{r}) = -\left( \frac{\alpha_2 e^2}{2r^4} + \frac{Q}{r^3} \right) P_2(\cos \theta) \quad (4)$$

and a short-range potential  $V_S(r)$ . The long-range potential is expressed in terms of the static spherical and non-spherical polarizabilities  $\alpha$  and  $\alpha_2$ , respectively, and the quadrupole moment  $Q$ . The short-range part  $V_S(r)$  comes into play at the distances comparable to the size of the molecule, where the molecule cannot be treated as a single object. Numerous approaches were proposed in the past, based on modifications of the polarization potential [3], deriving the short-range interaction from electronic densities etc. [34], or expanding the scattering amplitude at low energies [33]. In the present approach we express  $V_S(r)$  in terms of some boundary conditions imposed on the wave function at  $r \rightarrow 0$ , while the effects resulting from the finite range of  $V_S(r)$  are included explicitly in the framework of the modified effective-range theory.

In the following we assume that the nonisotropic part  $V_2(\mathbf{r})$  can be neglected in comparison to the isotropic polarization potential  $V_1(\mathbf{r})$ . This is justified as long as the quadrupole moment  $Q$  and the nonspherical polarizability  $\alpha_2$  expressed in atomic units are much smaller than  $\alpha$ .

In such a case the main effect of the non-isotropic terms is the coupling between different partial waves, while their contribution to the total cross-section at low energies remains small. As we show later in Section 5, where we analyze the corrections arising from  $V_2(\mathbf{r})$ , this is a good approximation in the case of N<sub>2</sub> molecules.

The radial part of the Schrödinger equation with the isotropic polarization potential  $V_l(\mathbf{r})$  reads

$$\left[ \frac{\partial^2}{\partial r^2} - \frac{l(l+1)}{r^2} + \frac{(R^*)^2}{r^4} + \frac{2\mu E}{\hbar^2} \right] \Psi_l(r) = 0, \quad (5)$$

where  $\Psi_l(r)$  denotes the radial wave function for the partial wave  $l$ . For the polarization potential, it is convenient to introduce some characteristic units  $R^*$  and  $E^*$ , where  $R^* \equiv \sqrt{\alpha e^2 \mu / \hbar^2}$  denotes the characteristic length of the  $r^{-4}$  potential, and  $E^* = \hbar^2 / (2\mu R^{*2})$  is the characteristic energy. With appropriate change of variables, the Schrödinger equation (5) can be transformed into Mathieu's differential equation of the imaginary argument [11,35,36], and solved analytically in terms of the continued fractions. Some basic properties of the analytical solutions are discussed in Appendices A–C (see [37,38] for more details on Mathieu functions). Here, we focus only on the behavior at small and large distances. For  $r \ll R^*$ , when the polarization potential dominates over centrifugal potential and the constant energy term, behavior of  $\Psi_l(r)$  is given by

$$\Psi_l(r) \stackrel{r \rightarrow 0}{\sim} r \sin\left(\frac{R^*}{r} + \phi_l\right), \quad (6)$$

where  $\phi_l$  is a short-range phase, which is determined by  $V_S(r)$ . For  $E = 0$  and  $l = 0$  the solution (6) becomes exact at all distances, and from its asymptotic behavior at large distances one can easily determine the value of the  $s$ -wave scattering length

$$a_s = -R^* \cot(\phi_0). \quad (7)$$

At large distances:  $r \gg R^*$ ,  $\Psi_l(r)$  must take the form of the scattered wave

$$\Psi_l(r) \stackrel{r \rightarrow \infty}{\sim} \sin(kr - l\frac{\pi}{2} + \eta_l), \quad (8)$$

where  $k = \sqrt{2\mu E} / \hbar$ . Using the Mathieu functions one can find the following relation between the phase shift  $\eta_l$  and the short range phase  $\phi_l$  [11]

$$\tan \eta_l = \frac{m^2 - \tan^2 \delta + \tan(\phi_l + l\frac{\pi}{2}) \tan \delta (m^2 - 1)}{\tan \delta (1 - m^2) + \tan(\phi_l + l\frac{\pi}{2}) (1 - m^2 \tan^2 \delta)}, \quad (9)$$

where  $\delta = \frac{\pi}{2}(\nu - l - \frac{1}{2})$ , and  $m$  and  $\nu$  are some parameters, that are determined by the analytical solutions (see Appendices A and B for details).

In general, the parameter  $\phi_l$  entering the asymptotic formula (6), depends on energy, and can be expanded in powers of  $k$ . In our case it is more convenient to expand  $\tan(\phi_l + l\frac{\pi}{2})$ , entering formula (9):

$$\tan(\phi_l + l\frac{\pi}{2}) = A_l + \frac{1}{2} R^* R_l k^2 + \dots, \quad (10)$$

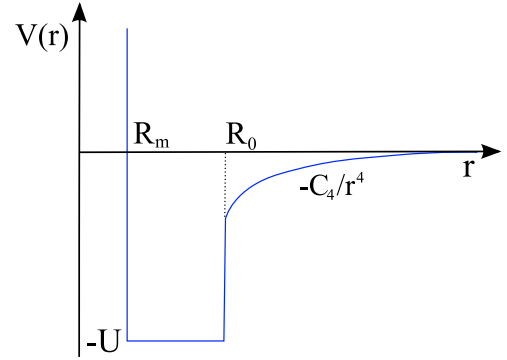


**Fig. 1.** The model potential equation (13) that is used to test MERT for the shape resonances.

where  $A_l \equiv \tan(\phi_l + l\frac{\pi}{2})|_{q=0}$ . The lowest order correction in  $k$  is quadratic, and can be interpreted as an effective range  $R_l$  for the partial wave  $l$  [11].

Combining (9), (10), (34), (35) one can easily obtain the low-energy expansion of the phase shifts [11]

$$q \cot \eta_0 = -\frac{1}{a} + \frac{\pi}{3a^2} q + \frac{4}{3a} \ln\left(\frac{q}{4}\right) q^2 + \frac{R_0^2}{2} q^2 + \left[ \frac{\pi}{3} + \frac{20}{9a} - \frac{\pi}{3a^2} - \frac{\pi^2}{9a^3} - \frac{8}{3a} \psi\left(\frac{3}{2}\right) \right] q^2 + \dots \quad (11)$$

$$\tan \eta_l = \frac{\pi q^2}{8(l - \frac{1}{2})(l + \frac{1}{2})(l + \frac{3}{2})} + \dots, \quad l \geq 1 \quad (12)$$

here,  $q = kR^*$ , and  $a = a_s/R^* = -1/A_0$ . The low-energy expansions (11)–(12) are applicable only at small energies  $E \ll E^*$ . In contrast, in our approach we use the exact formula (9) for the phase shift, with the short-range phase expanded according to (10).

### 3 Model calculation

To illustrate how MERT works for the low-energy scattering on the long-range  $r^{-4}$  potential we consider a simple model of the potential with a square-well interaction at short distances (see Fig. 1)

$$V(r) = \begin{cases} \infty & r < R_m \\ -U & R_m < r < R_0 \\ -C_4/r^4 & r > R_0 \end{cases} \quad (13)$$

here,  $R_m$  denotes a hard-core radius and  $R_0$  is the radius of the square-well potential. The potential  $V(r)$  does not reproduce the full behavior of the electron-molecule interaction, however, it captures the basic properties of shape resonances in such a system, and allows to verify the accuracy of our MERT-based approach. The Schrödinger equation for the potential  $V(r)$  and partial-wave quantum

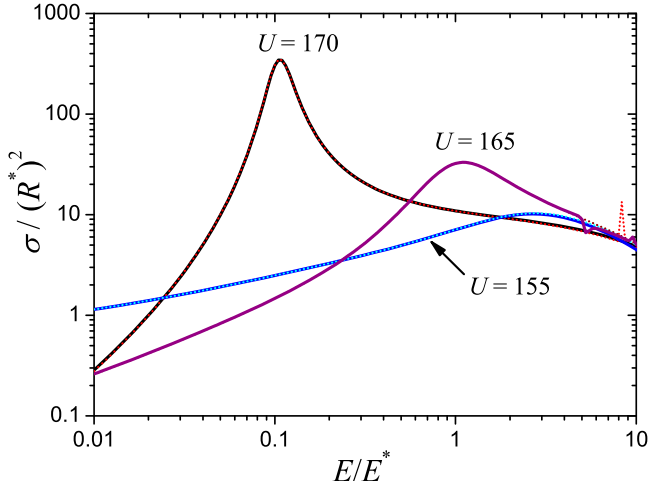


**Fig. 2.** (Color online) Total elastic cross-section versus energy for the scattering in the model potential (13), calculated for  $R_m = 0.1 R^*$ ,  $R_0 = 0.5 R^*$  and for different depths  $U$  of the square-well potential. The exact results for this model potential (solid lines) are compared with predictions of MERT (dotted lines, indistinguishable on the scale of figure) including terms up to  $q^2$  for the short-range part of the potential. Results are scaled by the the characteristic distance  $R^*$  and the characteristic energy  $E^*$  of the polarization potential.

number  $l$  can be solved exactly:

$$\Psi(r) = \begin{cases} 0 & r < R_m \\ r j_l(\chi r) + C(E) r n_l(\chi r) & R_m < r < R_0 \\ A(E) \sqrt{r} M_\nu(z) + B(E) \sqrt{r} T_\nu(z) & r > R_0 \end{cases} \quad (14)$$

where  $z = \ln(\sqrt{R^*}/\sqrt{kr})$ ,  $\hbar^2 \chi^2 / (2\mu) = E + U$ ,  $j_l(x)$  and  $n_l(x)$  denote spherical Bessel functions, and  $M_\nu(z)$  and  $T_\nu(z)$  are the two linearly independent solutions for  $r^{-4}$  potential. Parameters  $A(E)$ ,  $B(E)$ , and  $C(E)$  are to be determined from the continuity conditions for  $\Psi(r)$  at  $r = R_m$  and  $r = R_0$ . With the help of the asymptotic formulas (30) and (31) for  $M_\nu(z)$  and  $T_\nu(z)$  for large and negative argument  $z$  (large  $r$ ) we find exact phase shifts and the total cross-section for scattering on  $V(r)$ .

We compare the exact result with our MERT model, where MERT parameters  $A_l$  and  $R_l$  are determined from the expansion of the short range phase  $\phi_l$ . To this end we compare the form of the wave function (14) for  $r > R_0$ , with the solution (33) derived in Appendix B, obtaining the following condition for  $\phi_l$ :  $\tan(\phi_l(E) + \frac{\pi}{2}\nu(E) + \frac{\pi}{4}) = A(E)/B(E)$ . Expanding of  $A(E)$ ,  $B(E)$  and  $\nu(E)$  in powers of  $k$  (cf. (34)) yields  $A_l$  and  $R_l$ .

Figure 2 shows the dependence of the total elastic cross-section on energy, for few particular values of  $U$ , for which  $p$ -wave shape-resonances appear. The range  $R_0$  was chosen to be smaller than  $R^*$ , but still, of the same order as  $R^*$ , that roughly corresponds to the conditions of the low-energy electron(positron)-molecule scattering. The resonances show up as peaks at some particular values of the energy. We observe that MERT, including only two

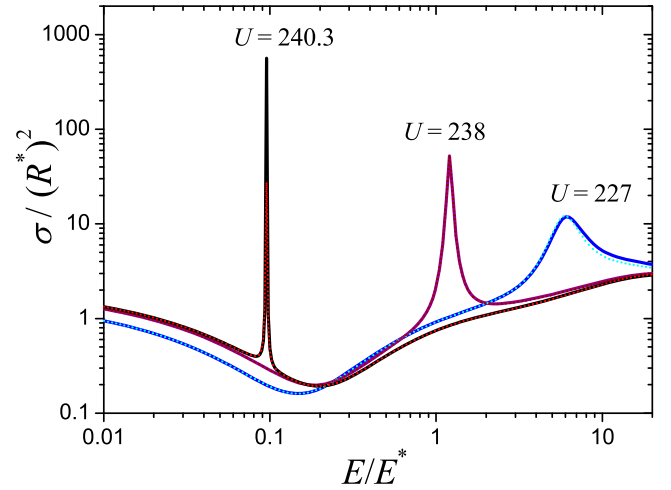


**Fig. 3.** (Color online) Same as Figure 2, but for values of  $U$  for which shape resonances in  $d$  wave appear.

lowest expansion coefficients  $A_l$  and  $R_l$  of the short-range potential, reproduces very accurately the exact results. The accuracy decreases for higher energies, where one can observe some discrepancies, in particular small peaks corresponding to the  $g$ -wave resonances that appear at different energies for exact and MERT curves. This results from higher sensitivity of the quasi-bound states on the parameters of the short-range potential for larger  $l$ , and the absence of the higher order terms in expansion (10) when  $E$  becomes too large. Nevertheless, the approximate MERT treatment remains very accurate for the main resonances in  $p$ -wave channel, even for energies significantly larger than  $E^*$ . Although, for relatively deep potentials considered here, the perfect agreement between the exact and MERT results is rather expectable, we have verified that MERT remains quite accurate, even for much weaker square well potentials, where the quasi-bound states extends well beyond  $R_0$ .

A similar comparison, but for  $d$ -wave resonances is presented in Figure 3. In this case the resonance peaks are narrower due to the stronger centrifugal barrier, and weaker coupling between quasi-bound and scattering states. Again, the agreement between MERT and the exact results is very good, and some discrepancies can be observed only at  $E \sim 10 E^*$ . Finally, we note that for  $l = 2$  and parameters of Figure 3 the quasi-bound state is totally localized within the range of the short-range potential. This shows that MERT is able to reproduce well the low energy behavior of the total cross-sections, including the regime of the shape resonances resulting solely from the short-range potential, even if the latter is treated in terms of an effective-range expansion. The reason why MERT works up to energies much higher than  $E^*$  can be understood on the basis of the shape-independent condition  $k \ll 1/R_0$  for the short range potential, that estimates the regime when the short-range phases  $\phi_l$  are energy independent. For  $R_0 \approx 0.5 R^*$ , this leads to the condition  $E \ll 4 E^*$ , which is shifted to higher energies, by inclusion of the effective-range term  $\frac{1}{2} R^* R_l k^2$  in the expansion (10).

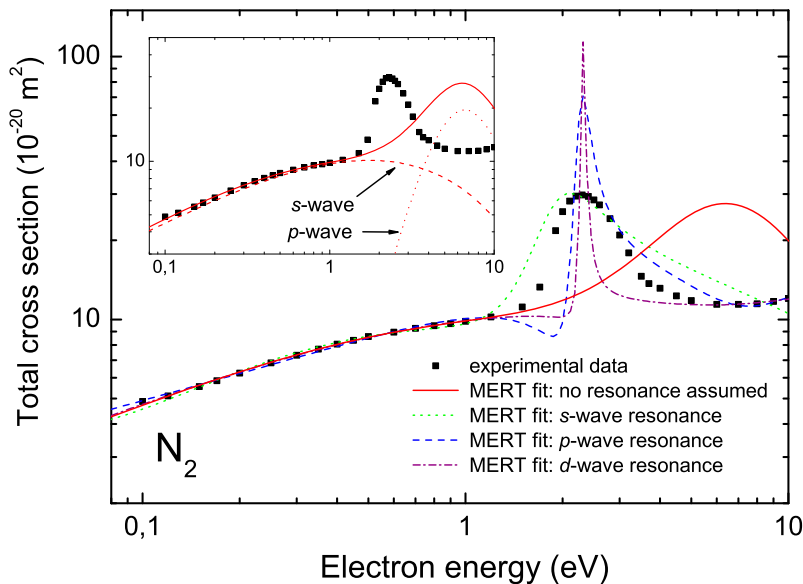


**Fig. 4.** (Color online) Total cross-section for the scattering of electrons on N<sub>2</sub> versus the energy. Depicted are: recommended experimental data from review [16] (squares), the theoretical fits based on MERT, assuming the resonance ( $\tan \eta_l = \pi/2$ ) at 2.1 eV in  $s$  wave (dotted line),  $p$  wave (dashed line), and  $d$  wave (dot-dashed line), and without assumption with respect to the position of the resonance (solid line). The inset shows in addition the  $s$ -wave and  $p$ -wave contributions to the MERT fit not assuming the position of resonance.

#### 4 MERT analysis of low-energy electron scattering

We investigate the low-energy electron scattering on N<sub>2</sub> molecule using a theoretical model based on MERT for  $s$  and  $p$  partial waves [10]. Our model contains four unknown parameters: the scattering length  $a = a_s/R^* = -1/A_0$  and the effective range  $R_0$  for  $s$  wave, and the zero-energy contribution  $A_1$  and the effective range  $R_1$  for  $p$  wave, that are determined by fitting to the experimental data. In this way for  $l = 0$  and  $l = 1$  we neglect corrections of the order higher than  $k^2$  in expansion (10). On the other hand, for partial waves with  $l \geq 2$  we include only the lowest-order contribution to the scattering phase shifts that are due to the long-range polarization potential (12). This is sufficient as long as the energy  $E$  remains smaller than the centrifugal barrier, that for  $l = 2$  has height of  $9E^*$ . The total elastic cross-section  $\sigma(k) = 4\pi k^{-2} \sum_l \sin^2 \eta_l(k)$  is determined from the phase shifts (9) and (12), with  $\nu$  and  $m$  evaluated numerically, using the procedure described in Appendices A and B.

In the calculations we use recent experimental values of the polarizability, as measured in electron scattering experiments:  $\alpha = 11.54a_0^3$  [39]. First, we fit our model by the least-square, not weighted method to the experimental data exclusively below the resonances, i.e. for energies  $E \leq 1.2$  eV, down to the lowest energies available from beam experiments [16]. The fitted parameters from this check are listed in Table 1. Note, that the scattering potential parameters are expressed in characteristic distance units. For example, the scattering length  $a_s$  amounts to 0.404 atomic units, close to the value of 0.420 a.u. derived by Morrison et al. [17]. Subsequently, we extend MERT analysis, using the fitted parameters to higher energies. Figure 4 compares the experimental data (points) with the theoretical curves obtained from this fit (solid lines). This leads to the resonance maximum in the scattering cross-section, that is located at somewhat higher energies that

**Table 1.** Characteristic distance  $R^*$ , characteristic energy  $E^*$  and four fitting parameters:  $a = a_s/R^*$  ( $s$ -wave scattering length),  $A_1$  (zero-energy contribution from the short-range potentials for  $p$ -wave),  $R_0$  ( $s$ -wave effective range), and  $R_1$  ( $p$ -wave effective range) in the case of unconstrained fits and using only the very low energy experimental data.

|                | $R^*(a_0)$ | $E^*(\text{eV})$ | $a$   | $A_1$  | $R_0/R^*$ | $R_1/R^*$ |
|----------------|------------|------------------|-------|--------|-----------|-----------|
| N <sub>2</sub> | 3.397      | 1.179            | 0.119 | -0.537 | 0.110     | 0.262     |

the experimental one (at 2.1 eV). This “spontaneously” appearing resonance is due to the  $p$ -wave, see inset in Figure 4.

The range of fitted data corresponds to quite low energies in terms of characteristic units:  $E \lesssim E^*$ . Therefore, the fitting procedure, within the error bar of experimental points, is not able to predict with sufficient accuracy the cross-section in the energy range corresponding to resonance peaks. Also, neglectation of the nonisotropic part of the potential leads to some additional errors. Moreover, our scheme neglects the possibility of  $d$ -wave or higher partial wave resonances, that can be suggested e.g. by the behavior of differential cross-section for the scattering on N<sub>2</sub>. To eliminate these shortcomings we have subsequently added to the fitting procedure also some experimental points, located in the energy range above the resonance:  $6 \text{ eV} < E < 10 \text{ eV}$ . In addition we have considered three possible scenario assuming that resonance maxima occur in partial waves  $s$ ,  $p$  or  $d$ , exactly at the energy of the resonance peak observed in the experimental data. This corresponds to the requirement that the phase shift  $\eta_l$  assumes value  $\pi/2$  at the peak location for  $l = 0, 1, 2$ , respectively. In this way we obtain some constrains on the six fitting parameters:  $a$ ,  $A_1$ ,  $A_2$  (zero-energy contributions) and  $R_0$ ,  $R_1$  and  $R_2$  (effective ranges). The results are shown in Figure 4, presenting apart from the previous

**Table 2.** Six fitting parameters:  $a = a_s/R^*$  ( $s$ -wave scattering length),  $A_1$  (zero-energy contribution for  $p$ -wave),  $A_2$  (zero-energy contribution for  $d$ -wave),  $R_0$  ( $s$ -wave effective range),  $R_1$  ( $p$ -wave effective range) and  $R_2$  ( $d$ -wave effective range) in the case of fits assuming resonances ( $\tan \eta_l = \pi/2$ ) in  $s$ ,  $p$  and  $d$  wave. The fits are made to the data below and above the experimentally observed resonance (see text for details). Note that for  $s$ -wave only four parameters (two partial waves) were sufficient to fit the data.

| $l$ | $a$    | $A_1$  | $A_2$  | $R_0/R^*$ | $R_1/R^*$ | $R_2/R^*$ |
|-----|--------|--------|--------|-----------|-----------|-----------|
| 0   | -0.447 | -0.021 | -      | -3.100    | -0.104    | -         |
| 1   | 0.157  | -4.314 | -0.130 | -47.05    | 4.704     | 0.079     |
| 2   | 0.123  | -0.390 | -0.222 | -0.301    | -0.174    | 0.293     |

data, also theoretical curves with maxima assumed in  $s$ ,  $p$  and  $d$  wave. The fitted parameters are listed in Table 2.

We observe that the height of the resonance peak for  $s$  wave agrees well with the experimental data (we show experimental values averaged over the vibrational structure seen in the resonance, following recommended data from Ref. [16]). This would suggest a possible  $s$ -wave origin of the maximum. But this point requires some more detailed discussion.

As said before, the generally accepted classification of resonances describes “shape” resonances as occurring within the shape of the effective potential, formed from the static and polarization contributions with the centrifugal barrier added. Obviously, for the  $s$ -wave the centrifugal barrier does not exist so trapping of the electron within the shape of the effective potential is impossible. However, our calculations show a quick change in the  $s$ -wave phase shift, occurring approximately in the region of the experimentally observed resonance. On the other hand, assumption of resonances in  $p$  and  $d$  waves would lead to much narrower and higher peaks in the total cross-section than the experimental values. Therefore, a simple interpretation of the the  $N_2$  resonance is not easy: (i) elastic differential cross-sections at the resonance maximum (2.47 eV) show a dominating  $p$ -wave contribution; (ii) differential cross-sections for the first vibrational excitation ( $\nu = 0-1$ ) at 2.45 eV show almost a perfect  $d$ -wave dependence [40] while (iii) the MERT analysis does not exclude  $s$ -wave origin of the maximum in the cross-section. Clearly, several partial waves contribute to the resonance and our fairly simplified MERT analysis is not able to separate these contributions.

## 5 Corrections due to the nonisotropic part of the long-range potential

Already early works stressed the importance of other, apart from the spherical polarization, components of the long-range potential in the electron-molecule scattering. For  $N_2$ , non-spherical polarizability is rather strong (see Tab. 3), therefore it is necessary to evaluate corrections arising from the anisotropic part of the potential. In this section we calculate them, showing that they can be safely

**Table 3.** Parameters of the long-range potential  $V_L(\mathbf{r})$  for  $N_2$  molecule considered in our analysis. For  $\alpha$  we use recent experimental values of [39], and for  $\alpha_2$  and  $Q$  we use experimental values used in reference [17].

|       | $\alpha(a_0^3)$ | $\alpha_2(a_0^3)$ | $Q(ea_0^2)$ |
|-------|-----------------|-------------------|-------------|
| $N_2$ | 11.54           | 3.08              | -1.09       |

neglected in comparison to the leading contribution from the spherical polarizability.

In the present analysis we treat the quadrupole and non-spherical polarizability contributions together, but using two distinct methods for the zero-energy limit and at low  $E \sim E^*$  energies. To analyze the contribution from the nonisotropic part of the potential at very low energies ( $E \ll E^*$ ), we can compare the small- $k$  series expansions for the whole potential  $V_1(r) + V_2(r)$  [41], to the expansion including the spherical part  $V_1(r)$  only. For the isotropic part, the total cross-section can be obtained from expansions of the phase shifts given by equations (11), (12). Substituting the parameters of the potential listed in Table 3 one obtains

$$\frac{\sigma_{N_2}(q)}{4\pi} = a^2 + 24.60qa + 31.32q^2 \log(q)a^2 + O(q^3). \quad (15)$$

On the other hand, application of the small- $k$  expansion for the full potential [41] leads to

$$\begin{aligned} \frac{\sigma_{N_2}(q)}{4\pi} = & a^2 + 24.93qa + 0.23q + 0.11 \\ & + 31.63(a - 0.15)(a + 0.16)q^2 \log(q) + O(q^3). \end{aligned} \quad (16)$$

We observe that for the typical scales of the scattering length  $a \sim 1$ , the differences in the coefficients of equation (16) and equation (15) are at most of the order of 10%.

For higher energies  $E \sim E^*$  the importance of the nonisotropic part can be assessed with the help of the distorted wave approximation [42]. This technique is similar to the standard Born expansion of the scattering amplitude, and is based on the assumption that the total potential can be split into a strong part  $V_1$ , that is treated exactly, and the remaining contribution  $V_2$ , that is treated in the perturbative manner. In contrast to the Born approximation, where the expansion is done around the free-space solutions, here the expansion is performed around the scattering solution in the presence of  $V_1$ . The scattering amplitude can be written as a sum of the contributions from  $V_1$  and  $V_2$  separately (see e.g. [43])

$$f(\mathbf{k}_f, \mathbf{k}_i) = -\frac{m}{2\pi\hbar^2} (\langle \mathbf{k}_f | V_1 | \Phi^+(\mathbf{k}_i) \rangle + \langle \Phi^-(\mathbf{k}_f) | V_2 | \Psi^+ \rangle), \quad (17)$$

where  $\Phi^\pm(\mathbf{k})$  is the scattering state for the isotropic part  $V_1$

$$\Phi^\pm(\mathbf{k}) = e^{i\mathbf{k}\mathbf{r}} + G_0^\pm V_1 \Phi^\pm(\mathbf{k}), \quad (18)$$

$G_0^\pm$  is the free propagator

$$G_0^\pm = \lim_{\epsilon \rightarrow 0} (E - \mathbf{p}^2/2m \pm i\epsilon)^{-1}, \quad (19)$$

**Table 4.** The total elastic cross-section  $\sigma_0$  and corrections due to the nonspherical part of the long-range potential in N<sub>2</sub> molecule, for different energies  $E$  of the scattered electron and different short-range cut-off parameters  $R_0$ .

| $E/E^*$ | $\sigma_0$ | $R_0 = 0.5 R^*$ | $R_0 = 0.75 R^*$ | $R_0 = R^*$ |
|---------|------------|-----------------|------------------|-------------|
| 1.0     | 3.145      | 0.0306          | 0.0311           | 0.0300      |
| 2.0     | 4.014      | 0.0147          | 0.0135           | 0.0138      |
| 4.0     | 7.428      | 0.0059          | 0.0052           | 0.0053      |

and  $\Psi^+$  is the scattering state for the full potential, satisfying the following Lippmann-Schwinger equation

$$\Psi^+ = \Phi^+(\mathbf{k}_i) + G_1^+ V_2 \Psi^+, \quad (20)$$

$$G_1^+ = \lim_{\epsilon \rightarrow 0} (E - \mathbf{p}^2/2m - V_1 + i\epsilon)^{-1}. \quad (21)$$

The second term in equation (17) can be written in the form of a Born series

$$\langle \Phi^-(\mathbf{k}_f) | V_2 | \Psi^+ \rangle = \langle \Phi^-(\mathbf{k}_f) | V_2 + V_2 G_1^+ V_2 + \dots | \Phi^+(\mathbf{k}_i) \rangle. \quad (22)$$

Finally, to calculate the total cross-section we apply the optical theorem:  $\sigma = \frac{4\pi}{k} \text{Im} f(\mathbf{k}_i, \mathbf{k}_i)$  [42].

Taking into account averaging over isotropic distribution of the molecule orientations in the sample, one can easily show that the lowest order contribution from  $V_2$ :  $\langle \Phi^-(\mathbf{k}_f) | V_2 | \Phi^+(\mathbf{k}_i) \rangle$  vanishes. Hence, for the small anisotropic part, the leading contribution is provided by the second order term  $\langle \Phi^-(\mathbf{k}_f) | V_2 G_1^+ V_2 | \Phi^+(\mathbf{k}_i) \rangle$ . We evaluate this term using analytical solutions for  $V_1$ , that both enter the scattering solution  $\Phi^\pm(\mathbf{k})$ , and the Green function  $G_1^+$ . The latter is expressed in terms of partial wave expansion including radial solutions for the  $V_1$  potential [42]. Because of the singular character of the long-range potential at  $r = 0$ , the second order corrections diverges at  $r \rightarrow 0$ , and we introduce an additional cut-off parameter  $R_0$  in the integration at short distances. Physically,  $R_0$  describes the distance when the interaction potential takes a form of the long range potential  $V_1 + V_2$ , which is roughly of the size of the molecule.

Table 4 lists the the corrections due to the nonisotropic part  $V_2$ , together with total cross-sections coming from the isotropic part  $V_1$ . The analytical unperturbed solution for  $V_1$  was calculated for parameters of Table 1, corresponding to the low-energy unconstrained fits. We observe that the corrections are small, of the order of 1%, and in principle, they slightly depend on the cut-off parameter  $R_0$ . The latter is a consequence of the fact that the analytical solutions for the pure polarization potential  $V_1$  become not physical at small distances, where the short-range part of the potential comes into play. Therefore corrections listed in Tables 4 estimate contributions of  $V_2$  from large distances only, where the potential takes the asymptotic form  $V_1 + V_2$ . On the other hand, we know that at short distances the anisotropic contributions in this region are not important, since the interaction potential is mainly determined by the short-range molecular forces.

## 6 Conclusions

MERT analytical solution was applied previously [10] for positron scattering cross-sections. In general, positron-scattering cross-sections in the limit of low energies fall monotonically with rising energy, up to the positronium formation threshold, and do not exhibit particular structures, see [44]. The model [10] approximated well Ar and N<sub>2</sub> integral elastic cross-sections at 0–2 eV. The derived scattering potentials were characterized by negative values of the scattering length-like parameters:  $a$  and  $A_1$ , for  $s$  and  $p$  waves, respectively.

At present, we have applied the MERT analysis to electron scattering on N<sub>2</sub> molecule. Parameters of the short range potential (the scattering length and the effective range) for the  $s$ ,  $p$ , and for higher energies also  $d$  partial wave, were obtained via fitting procedures using low-energy experimental data. The model approximates well the experimental data up to about 1–2 eV and the deduced value of the  $s$ -wave scattering length agrees well with the values known in the literature.

Deriving the potential parameters from the experimental data below resonance and using them again for our model at higher energy, we obtained  $p$ -wave resonances, although at slightly higher energies than observed experimentally. To check for the consistency of the fit, the model was applied jointly to the data below and above resonance, assuming that the resonance occur in the  $s$ ,  $p$  or  $d$  wave, at the energy as observed experimentally. Within the latter constraint, a “resonance-like” peak, corresponding to the  $\pi/2$  phase change appears also in the  $s$ -wave channel. In that case the peak is not as sharp as pure shape resonances in  $p$  and  $d$  partial waves.

As far as amplitude are considered, fixing the resonance position reproduces well the absolute value of the total cross-section in its maximum, but only if the resonance is assumed to appear in the  $s$ -wave channel. This seems somehow surprising, as the N<sub>2</sub> low-energy resonance is usually classified as the  $^2\Pi_u$  state. However, the extended calculations by Sun et al. [13] showed that “elastic resonant integral cross-sections entail comparable contributions from the  $^2\Pi_g$  and the  $^2\Sigma_g$  transition matrices [...]”. These authors [13] showed also that even if a few partial waves allow to reproduce the shape of differential cross-sections, as many as 13 of them are needed in the resonance to reproduce the absolute values of cross-sections.

More experimental points at low energies, would be useful for MERT modelling. We recall here Ramanan and Freeman [45] who on the basis of their swarm experiment stated: “experimental data presently available do not rule out the existence of a Ramsauer-Townsend minimum at an electron energy of 0.4 meV or lower”.

Summarizing, the present work unifies in a single model the very low-energy dependence of the integral cross-sections in N<sub>2</sub> with the occurrence of shape resonances at a few eV energies. It confirms that limitations on applicability of MERT to the very low energy range, come rather from direct expansions of the phase-shifts in series of  $k$ , rather than from any intrinsic defects of the effective range model. Obviously, several aspects of

resonant scattering, like partitioning between the elastic and vibrational/rotational excitation are beyond the capacities of our model. It would be challenging to incorporate MERT potentials to more advanced theoretical treatments, in particular of inelastic direct and resonant scattering [46–48].

The authors thank L.P. Pitaevskii for stimulating discussions. One of the author (Z.I.) acknowledges support of the Polish Government Research Grant for 2007-2010.

## Appendix A: Solutions of the Schrödinger equation for $1/r^4$ potential

The method for solving the Schrödinger equation with the polarization potential was discussed in our previous paper [10]. Below we indicate the basic steps of the derivation. In the radial Schrödinger equation (5) we substitute  $r = \sqrt{R^*}e^{-z}/\sqrt{k}$  and  $\Psi_l(r) = \psi(r)\sqrt{r/R^*}$ , which yields the Mathieu's modified differential equation [37,38]

$$\frac{d^2\psi}{dz^2} - [a - 2q \cosh 2z] \psi = 0, \quad (23)$$

where  $a = (l + \frac{1}{2})^2$  and  $q = kR^*$ . Two linearly independent solutions  $M(z)$  and  $T(z)$  can be expressed in the following form [36,37]

$$M_\nu(z) = \sum_{n=-\infty}^{\infty} (-1)^n c_n(\nu) J_{2n+\nu}(2\sqrt{q} \cosh z), \quad (24)$$

$$T_\nu(z) = \sum_{n=-\infty}^{\infty} (-1)^n c_n(\nu) Y_{2n+\nu}(2\sqrt{q} \cosh z), \quad (25)$$

here,  $\nu$  denotes the characteristic exponent, and  $J_\nu(z)$  and  $Y_\nu(z)$  are Bessel and Neumann functions respectively. Substituting the ansatz (24) and (25) into (23) one obtains the following recurrence relation:

$$[(2n + \nu)^2 - a] c_n + q(c_{n-1} + c_{n+1}) = 0, \quad (26)$$

which can be solved in terms of continued fractions. To this end we introduce  $h_n^+ = c_n/c_{n-1}$  and  $h_n^- = c_{-n}/c_{-n+1}$  for  $n > 0$ , which substituted into (26) gives the continued fractions

$$h_n^+ = -\frac{q}{qh_{n+1}^+ + d_n}, \quad h_n^- = -\frac{q}{qh_{n+1}^- + d_{-n}}, \quad (27)$$

with  $d_n = (2n + \nu)^2 - a$ . Characteristic exponent has to be determined from equation (26) for  $n = 0$  expressed in terms of  $h_1^-$  and  $h_1^+$ . In practice, to find numerical values of the coefficients  $c_n$  we set  $h_m^+ = 0$  and  $h_m^- = 0$  for some, sufficiently large  $m$  and calculate  $h_n^+$  and  $h_n^-$  up to  $n = 1$  using (27).

## Appendix B: Asymptotic expansions for large arguments

Asymptotic behavior of  $M_\nu(z)$  and  $T_\nu(z)$  for large  $z$  follows immediately from asymptotic expansions of Bessel functions for large arguments [38]

$$M_\nu(z) \xrightarrow{z \rightarrow \infty} \sqrt{\frac{2}{\pi}} \frac{e^{-z/2}}{q^{1/4}} s_\nu \cos\left(e^z \sqrt{q} - \frac{\pi}{2}\nu - \frac{\pi}{4}\right) \quad (28)$$

$$T_\nu(z) \xrightarrow{z \rightarrow \infty} \sqrt{\frac{2}{\pi}} \frac{e^{-z/2}}{q^{1/4}} s_\nu \sin\left(e^z \sqrt{q} - \frac{\pi}{2}\nu - \frac{\pi}{4}\right) \quad (29)$$

where  $s_\nu = \sum_{n=-\infty}^{\infty} c_n(\nu)$ . To obtain asymptotic behavior for large and negative  $z$  it is necessary to connect solutions  $M_\nu(z)$  and  $T_\nu(z)$ , with another pair of solution  $M_\nu(-z)$  and  $T_\nu(-z)$  across  $z = 0$  [36]. In this way one obtains [10]

$$M_\nu(z) \xrightarrow{z \rightarrow -\infty} \sqrt{\frac{2}{\pi}} \frac{e^{z/2}}{q^{1/4}} m s_\nu \cos\left(\sqrt{q}e^{-z} + \frac{\pi}{2}\nu - \frac{\pi}{4}\right) \quad (30)$$

$$T_\nu(z) \xrightarrow{z \rightarrow -\infty} -\sqrt{\frac{2}{\pi}} \frac{e^{z/2}}{q^{1/4}} \frac{s_\nu}{m} \left[ \sin\left(\sqrt{q}e^{-z} + \frac{\pi}{2}\nu - \frac{\pi}{4}\right) - \cot \pi\nu(m^2 - 1) \cos\left(\sqrt{q}e^{-z} + \frac{\pi}{2}\nu - \frac{\pi}{4}\right) \right] \quad (31)$$

where  $m = \lim_{z \rightarrow 0^+} M_\nu(z)/M_{-\nu}(z)$ . To evaluate  $m$  numerically, we rather avoid using formula (24), where summation over  $n$  converges very slowly for  $z \rightarrow 0$ . An alternative approach is to use a different representation for the solutions of the Mathieu's equation [37]

$$W_\nu(z) = \sum_{n=-\infty}^{\infty} c_n(\nu) e^{2n+\nu}, \quad (32)$$

where  $c_n(\nu)$  are the same coefficients as used in definition of  $M_\nu(z)$  and  $T_\nu(z)$ . One can show that  $W_\nu(z)$  differs from  $M_\nu(z)$  only by some constant prefactor. We utilize this fact calculating the prefactor at some moderate values of the argument ( $z \sim 1$ ), and then evaluate  $m$  using the function  $W_\nu(z)$ , that has well defined behavior at  $z \rightarrow 0$ .

Finally the radial wave function  $\Psi_l(r)$  for partial wave  $l$  can be written as linear combination of  $M_\nu(z)$  and  $T_\nu(z)$

$$\Psi_l(r) = \sin\left(\phi_l + \frac{\pi}{2}\nu + \frac{\pi}{4}\right) \sqrt{\frac{R^*}{r}} M_\nu\left(\ln \frac{\sqrt{R^*}}{\sqrt{kr}}\right) + \cos\left(\phi_l + \frac{\pi}{2}\nu + \frac{\pi}{4}\right) \sqrt{\frac{R^*}{r}} T_\nu\left(\ln \frac{\sqrt{R^*}}{\sqrt{kr}}\right), \quad (33)$$

where  $\phi_l$  is a parameter which appear in the small  $r$  expansion (6). Now, the behavior of  $\Psi(r)$  at small and large distance described by equations (6)–(9), can be readily obtained from asymptotic expansions (28)–(31).

## Appendix C: Expansions for small energies

Behavior of the parameters  $m$  and  $\nu$  at small energies is given by the following series expansions [49]

$$\nu(q) = l + \frac{1}{2} - \frac{q^2}{4(l - \frac{1}{2})(l + \frac{1}{2})(l + \frac{3}{2})} + O(q^4), \quad (34)$$

and

$$m(q) = \left(\frac{q}{4}\right)^{l+\frac{1}{2}} \frac{\Gamma(\frac{1}{2} - l)}{\Gamma(\frac{3}{2} + l)} + O(q^{l+5/2}), \quad (35)$$

where  $\psi(x)$  denotes the digamma function [38]. The above formulas can be obtained, for instance, by solving the recurrence relation (26) keeping only the lowest-order terms:  $c_0$ ,  $c_{-1}$  and  $c_1$ .

## References

1. *Atomic and molecular processes: an R-matrix approach*, edited by P.G. Burke, K.A. Berrington (IOP, Bristol, 1993)
2. J. Tennyson, J.D. Gorfinkiel, I. Rozum, C.S. Trevisan, N. Vinci, *Radiat. Phys. Chem.* **68**, 65 (2003)
3. E. Czuchaj, J.E. Sienkiewicz, W. Miklaszewski, *Chem. Phys.* **116**, 69 (1987)
4. A.P.P. Natalense, M.H.F. Bettega, L.G. Ferreira, M.A.P. Lima, *Phys. Rev. A* **52**, R1 (1995)
5. W.A. Isaacs, C.W. McCurdy, T.N. Rescigno, *Phys. Rev. A* **58**, 309 (1998)
6. F.A. Gianturco, J.A. Rodriguez-Ruiz, *Phys. Rev. A* **47**, 1075 (1993)
7. F.A. Gianturco, R.R. Lucchese, N. Sanna, *J. Chem. Phys.* **104**, 6482 (1996)
8. F.A. Gianturco, D. De Fazio, J.A. Rodriguez-Ruiz, K.T. Tang, J.P. Toennies, *Z. Phys. D* **33**, 27 (1995)
9. F.A. Gianturco, P. Paoletti, J.A. Rodriguez-Ruiz, *Z. Phys. D* **36**, 51 (1996)
10. Z. Idziaszek, G. Karwasz, *Phys. Rev. A* **73**, 064701 (2006)
11. T.F. O'Malley, L. Spruch, L. Rosenberg, *J. Math. Phys.* **2**, 491 (1961)
12. Z. Idziaszek, G.P. Karwasz, R.S. Brusa, *J. Phys. Conf. Ser.* **115**, 012002 (2008)
13. W. Sun, M.A. Morrison, M.A. Isaacs, W.K. Trail, D.T. Alle, R.J. Gulley, M.J. Brennan, S.J. Buckman, *Phys. Rev. A* **52**, 1229 (1995)
14. Cz. Szmytkowski, K. Maciąg, G. Karwasz, *Phys. Scr.* **54**, 271 (1996)
15. S. Telega, F.A. Gianturco, *Eur. Phys. J. D* **38**, 495 (2006)
16. G.P. Karwasz, A. Zecca, R.S. Brusa, *Electron Scattering with Molecules*, in Landolt-Börstein New Series, *Photon and Electron Interaction, with Atoms, Molecules and Ions* (Springer-Verlag, Berlin, Heidelberg, 2003), Vol. I/17, pp. 6.1–6.51
17. M.A. Morrison, W. Sun, W.A. Isaacs, W.K. Trail, *Phys. Rev. A* **55**, 2786 (1997)
18. H.P. Saha, *Phys. Rev. A* **39**, 5048 (1989)
19. G.N. Haddad, T.F. O'Malley, *Austr. J. Phys.* **35**, 35 (1982)
20. T. Sasakawa, J. Horáček, *J. Phys. B* **15**, L169 (1982)
21. F.A. Gianturco, K. Willner, *Phys. Rev. A* **75**, 062714 (2007)
22. I.I. Fabrikant, H. Hotop, M. Allan, *Phys. Rev. A* **71**, 22712 (2005)
23. I.I. Fabrikant, *J. Phys. B: At. Mol. Phys.* **16**, 1269 (1983)
24. W. Vanroose, C.W. McCurdy, T.N. Rescigno, *Phys. Rev. A* **68**, 052713 (2003)
25. J. Ferch, B. Granitza, W. Raith, *J. Phys. B* **18**, L445 (1985)
26. A. Mann, F. Linder, *J. Phys. B* **25**, 533 (1992)
27. G.P. Karwasz, A. Karbowski, Z. Idziaszek, R.S. Brusa, *Nucl. Instrum. Meth. B* **266**, 471 (2008)
28. P.A. Macri, R.O. Barrachina, *Phys. Rev. A* **65**, 062718 (2002)
29. P.A. Macri, R.O. Barrachina, *Nucl. Instrum. Meth. B* **205**, 543 (2003)
30. S.J. Buckman, J. Mitroy, *J. Phys. B* **22**, 1365 (1989)
31. H.R. Sadeghpour, J.L. Bohn, M.J. Cavagnero, B.D. Esry, I.I. Fabrikant, J.H. Macek, A.R.P. Rau, *J. Phys. B* **33** R93 (2000)
32. S. Watanabe, Ch.H. Greene, *Phys. Rev. A* **22**, 158 (1980)
33. I.I. Fabrikant, *Opt. Spektrosk.* **53**, 223 (1982)
34. F.A. Gianturco, P. Paoletti, *Phys. Rev. A* **55**, 3491 (1997)
35. E. Vogt, G.H. Wannier, *Phys. Rev.* **95**, 1190 (1954)
36. R.M. Spector, *J. Math. Phys.* **5**, 1185 (1964)
37. A. Erdélyi, *Higher transcendental functions* (McGraw-Hill, New York, 1955), Vol. III
38. M. Abramowitz, I.A. Stegun, *Handbook of Mathematical Functions* (Dover, New York, 1972)
39. T.N. Olney, N.M. Cann, G. Cooper, C.E. Brion, *Chem. Phys.* **223**, 59 (1997)
40. M. Allan, *J. Phys. B: At. Mol. Phys.* **35**, L387 (2002)
41. I.I. Fabrikant, *J. Phys. B: At. Mol. Phys.* **17**, 4223 (1984)
42. N.F. Mott, H.S.W. Massey, *Theory of Atomic Collisions*, 3rd edition (Clarendon Press, Oxford, 1965)
43. D.P. Dewangan, H.R.J. Walters, *J. Phys. B: At. Mol. Phys.* **10**, 637 (1977)
44. G.P. Karwasz, D. Pliszka, A. Zecca, R.S. Brusa, *Nucl. Instrum. Meth. B* **250**, 666 (2005); G.P. Karwasz, R.S. Brusa, D. Pliszka, *Nucl. Instrum. Meth. B* **251**, 520 (2006)
45. G. Ramanan, G.R. Freeman, *J. Chem. Phys.* **93**, 3120 (1990)
46. T.N. Rescigno, D.A. Byrum, W.A. Isaacs, C.W. McCurdy, *Phys. Rev. A* **60**, 2186 (1999)
47. S. Mazevet, M.A. Morrison, L.A. Morgan, R.B. Nesbet, *Phys. Rev. A* **64**, 040701 (2001)
48. T.N. Rescigno, W.A. Isaacs, A.E. Orel, H.-D. Meyer, C.W. McCurdy, *Phys. Rev. A* **65**, 032716 (2002)
49. J. Meixner, F.W. Schafke, *Mathieusche Funktionen und Sphäroid Funktionen* (Springer, Berlin, 1954)